Memorandum

Datum: January 5, 2009

Von: B.M.Wojek
Telefon: +41 (0)56 310 5453
Raum: WLGA / 019
E-Mail: bastian.wojek@psi.ch

An: To whom it may concern

cc:

Four-point resistivity correction factors for thin films

In this memo a short review on the calculation of the resistivity of *homogeneous thin films* from four-point resistance measurements is given; it is mainly following arguments of Schroder [1] and Weller [2][1]. For the derivation of the proper resistivity correction factors we first assume a semi-infinite sample and then take subsequently the different geometrical boundary conditions into account.
Since we are dealing with four-point probe resistivity measurements, there are four contacts at the sample – two probes, say 1 and 4, where the current enters and leaves the sample and two probes, 2 and 3, between which the potential difference is measured.
In an semi-infinite sample with resistivity ρ the voltage V at a point at the distance r from a contact injecting the current I is given by

$$V = \frac{I\rho}{2\pi r}\,. \tag{1}$$

The total voltage at a voltage probe, e.g. probe 2, in the four-point geometry is therefore given by

$$V_2 = \frac{I\rho}{2\pi}\left(\frac{1}{r_{21}} - \frac{1}{r_{24}}\right)\,, \tag{2}$$

where r_{ab} is generally the distance between the contacts a and b. The minus sign accounts for the extracted current at probe 4.
Therefore, for any arrangement of the contacts, the potential difference between probes 2 and 3 is

$$\Delta V = V_2 - V_3 = \frac{I\rho}{2\pi}\left(\frac{1}{r_{21}} - \frac{1}{r_{24}} - \frac{1}{r_{31}} + \frac{1}{r_{34}}\right) \tag{3}$$

and the resistivity ρ becomes

$$\rho = \frac{2\pi}{1/r_{21} - 1/r_{24} - 1/r_{31} + 1/r_{34}}\frac{\Delta V}{I}. \tag{4}$$

If the probes are arranged on a line equidistantly (cf. Fig. 1 a)) with spacing s, equation 4 reduces to

$$\rho_{\mathrm{edl}} = 2\pi s\frac{\Delta V}{I}\,, \tag{5}$$

if one uses a standard square geometry (also with probe spacing s, cf. Fig. 1 b)), one gets

$$\rho_{\mathrm{sq}} = \frac{2\pi s}{2-\sqrt{2}}\frac{\Delta V}{I}\,, \tag{6}$$

and for the non-equidistant in-line geometry depicted in Fig. 1 c) the resistivity becomes

$$\rho_{\mathrm{nedl}} = \frac{6\pi s}{5}\frac{\Delta V}{I}\,. \tag{7}$$

[1] All cited references can be found on the NT-nemu-disk for internal use (NT-NEMU:\research related papers and talks\ThinFilmResistivity)

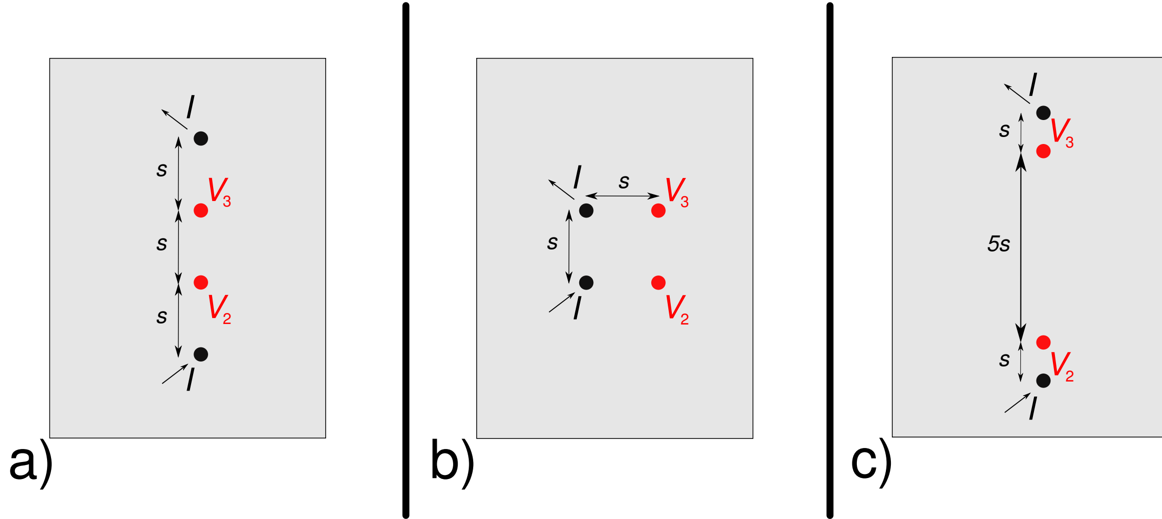

Figure 1: Sketches of the four-point probe geometries: a) equidistant in-line probes, b) square array probes, c) s–$5s$–s in-line probes

The formulae stated above are valid only for semi-infinite samples. Since real samples are thinner and have smaller lateral dimensions additional correction factors F are introduced and

$$\rho = \hat{s} F \frac{\Delta V}{I} \,, \tag{8}$$

where $\hat{s}$ is given by the different probe arrangements and equals the according coefficient in equations (5-7). There are different types of correction factors from which we are considering only three: F_1 accounts for the sample thickness, F_2 for the finite lateral dimensions and F_3 corrects for probe placement near the sample edges. In general these are considered to be independent and the total correction factor writes as

$$F = F_1 F_2 F_3. \tag{9}$$

In the following we will first concentrate on the factors F_1 and F_3 *only for non-conducting* substrates and boundaries and eventually derive one single factor taking into account all three corrections.

Thickness correction factor

For the collinear equidistant probe arrangement on a sample with thickness t Albers and Berkowitz introduced an analytical approximation for F_1 [4]:

$$F_{1,\mathrm{AB}} = \frac{t/s}{2\ln\left(\sinh\left(t/s\right)/\sinh\left(t/2s\right)\right)} \,, \tag{10}$$

which even reduces to

$$F_{1,\mathrm{AB}} \approx \frac{t/s}{2\ln\left(2\right)} \tag{11}$$

if the sample is much thinner than the probe spacing and the approximation $\sinh(t/s) \approx t/s$ holds. It should be emphasized again that these analytical forms are only valid for the equidistant in-line probe arrangement! To handle also other four-point geometries a more general approach described in some detail by Weller is needed [2]. In general Laplace's equation for the potential has to be solved with the boundary conditions given by the finite layer thickness. Albers and Berkowitz solved this problem [4] and the potential in the thin film ($0 \leqslant z \leqslant t$) as a function of the injected current I is given by

$$V(r,z) = \left(\frac{\rho I}{2\pi}\right) \int_0^\infty \left\{J_0(kr)\cdot\cosh(k(z-t)) - J_0(kr_0)\cdot\cosh(kt)\right\} \frac{dk}{\sinh(kt)} \,, \tag{12}$$

where J_0 is the 0th order Bessel function and $r = r_0$ specifies the circle on the surface ($z = 0$), where $V = 0$. Analogous to equation (2) for each voltage probe all the potential differences resulting from the different current injections and extractions have to be summed up. For an infinite thin layer this yields for the voltage between the probes 2 and 3

$$\begin{aligned} \Delta V(r_{21}, r_{24}, r_{31}, r_{34}, t) &= V_2 - V_3 \\ &= \left(\frac{\rho I}{2\pi}\right) \int_0^\infty \{J_0(kr_{21}) - J_0(kr_{24}) - J_0(kr_{31}) + J_0(kr_{34})\} \frac{\cosh(kt)}{\sinh(kt)} dk\,. \end{aligned} \tag{13}$$

The r_{ab} again denote the distances between the probes a and b. Since the surface of the thin layer is probed, z has been set to zero.
For the equidistant in-line geometry with probe distance s equation (13) reduces to

$$\Delta V(s, t) = \left(\frac{\rho I}{\pi}\right) \int_0^\infty \{J_0(ks) - J_0(2ks)\} \frac{\cosh(kt)}{\sinh(kt)} dk\,. \tag{14}$$

Introducing the new variables $\kappa \equiv ks$ and $\tau \equiv t/s$ equation (14) can be rewritten as

$$\Delta V(s, \tau) = \left(\frac{\rho I}{2\pi s}\right) \left(2 \int_0^\infty \{J_0(\kappa) - J_0(2\kappa)\} \frac{\cosh(\tau\kappa)}{\sinh(\tau\kappa)} d\kappa\right) \equiv \left(\frac{\rho I}{2\pi s}\right) f_{\text{edl}}(\tau)\,, \tag{15}$$

where it can be seen immediately that $1/f_{\text{edl}}(\tau) = F_{1,\text{edl}}$ in equations (8) and (9) since the corrections made by F_2 and F_3 have been neglected until now. The analytical approximation in equation (10) has in fact been derived by solving the integral (15). Valdes [3] gave a series representation of $f_{\text{edl}}(\tau)$, which is equivalent because of the following arguments given by Weller [2]. First, $f_{\text{edl}}(\tau)$ is rewritten as

$$f_{\text{edl}}(\tau) = 2 \int_0^\infty \{J_0(\kappa) - J_0(2\kappa)\} \left(\frac{\cosh(\tau\kappa)}{\sinh(\tau\kappa)} - 1\right) d\kappa + 2 \int_0^\infty \{J_0(\kappa) - J_0(2\kappa)\}\, d\kappa\,. \tag{16}$$

Using the identity $\int_0^\infty J_0(kr)dk = 1/r$ with[2] $r = 1$ and $r = 2$ and expressing the hyperbolic functions in terms of exponentials[3], equation (16) becomes

$$f_{\text{edl}}(\tau) = 1 + 4 \int_0^\infty \{J_0(\kappa) - J_0(2\kappa)\} \left(\frac{e^{-2\tau\kappa}}{1 - e^{-2\tau\kappa}}\right) d\kappa\,. \tag{17}$$

The last term in parenthesis can now be identified as geometrical series and the exchange of the order of summation and integration leads to

$$f_{\text{edl}}(\tau) = 1 + 4 \sum_{n=1}^\infty \left(\int_0^\infty \{J_0(\kappa) - J_0(2\kappa)\}\, e^{-2n\tau\kappa} d\kappa\right)\,. \tag{18}$$

The integral can now be solved analytically employing the identity

$$\int_0^\infty J_0(\alpha\kappa) e^{-\beta\kappa} d\kappa = \frac{1}{\sqrt{\alpha^2 + \beta^2}} \tag{19}$$

and $f(\tau)$ finally yields

$$f_{\text{edl}}(\tau) = 1 + 4 \sum_{n=1}^\infty \left(\frac{1}{\sqrt{1 + 4n^2\tau^2}} - \frac{1}{\sqrt{4 + 4n^2\tau^2}}\right)\,, \tag{20}$$

[2] Ref. [2] is wrong at this point; it is written "$k = 1$" and "$k = 2$" instead of "$r = 1$" and "$r = 2$"
[3] In Eqs. (14-15) of Ref. [2] the factor "2" is missing in every exponent.

which may be calculated numerically. Of course the above derivation was done exemplary for the in-line probe geometry, but can also be applied analogously to any other four-point geometry starting from equation (13). The result for the square geometry then is given by

$$\frac{1}{F_{1,\mathrm{sq}}} = f_{\mathrm{sq}}(\tau) = 1 + \frac{4}{2-\sqrt{2}} \sum_{n=1}^{\infty} \left(\frac{1}{\sqrt{1+4n^2\tau^2}} - \frac{1}{\sqrt{2+4n^2\tau^2}} \right) , \tag{21}$$

and for the non-equidistant in-line probe array the calculation yields

$$\frac{1}{F_{1,\mathrm{nedl}}} = f_{\mathrm{nedl}}(\tau) = 1 + \frac{12}{5} \sum_{n=1}^{\infty} \left(\frac{1}{\sqrt{1+4n^2\tau^2}} - \frac{1}{\sqrt{36+4n^2\tau^2}} \right) . \tag{22}$$

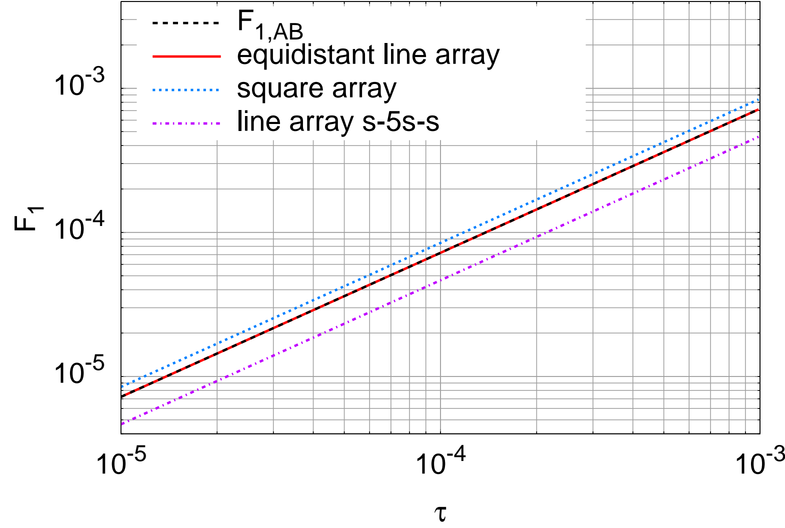

Figure 2: Thickness correction factors F_1 for the different probe geometries as a function of the normalized sample thickness $\tau = t/s$ according to Eqs. (20-22)

Correction for probing near the edge of a sample

The factor F_3 correcting for probing close to the edge of a sample is normally derived using the method of images. That means additional to the real current probes the voltage probes see superimposed mirrored currents originating from specular reflections at non-conducting boundaries as sketched in Fig. 3. As a result equation (3) then contains additional terms of the mirror currents. We are not going into the details of these calculations at this point but just give the results for the used standard geometries and the references where all the details of the calculations may be found.

For the equidistant in-line geometry parallel to an edge and the square geometry with the distance l to the edge and probe spacing s one finds [3]

$$\rho_{\mathrm{edl}} = \rho_{0,\mathrm{edl}} F_3(\lambda) = \rho_{0,\mathrm{edl}} \left(1 + \frac{2}{\sqrt{1+2\lambda^2}} - \frac{1}{\sqrt{1+\lambda^2}} \right)^{-1} \tag{23}$$

and [5]

$$\rho_{\mathrm{sq}} = \rho_{0,\mathrm{sq}} F_3(\lambda) = \rho_{0,\mathrm{sq}} \left(2-\sqrt{2} \right) \left(2 - \sqrt{2} + \frac{2}{1+2\lambda} - \frac{2}{\sqrt{1+(1+2\lambda)^2}} \right)^{-1} . \tag{24}$$

For the non-equidistant in-line geometry one obtains

$$\rho_{\mathrm{nedl}} = \rho_{0,\mathrm{nedl}} F_3(\lambda) = \rho_{0,\mathrm{nedl}} \left(1 + \frac{6}{5\sqrt{1+4\lambda^2}} - \frac{6}{5\sqrt{36+4\lambda^2}} \right)^{-1} , \tag{25}$$

where $\lambda = l/s$. $\rho_{0,\mathrm{edl}}$, $\rho_{0,\mathrm{sq}}$ and $\rho_{0,\mathrm{nedl}}$ are given by the equations (5-7) respectively.

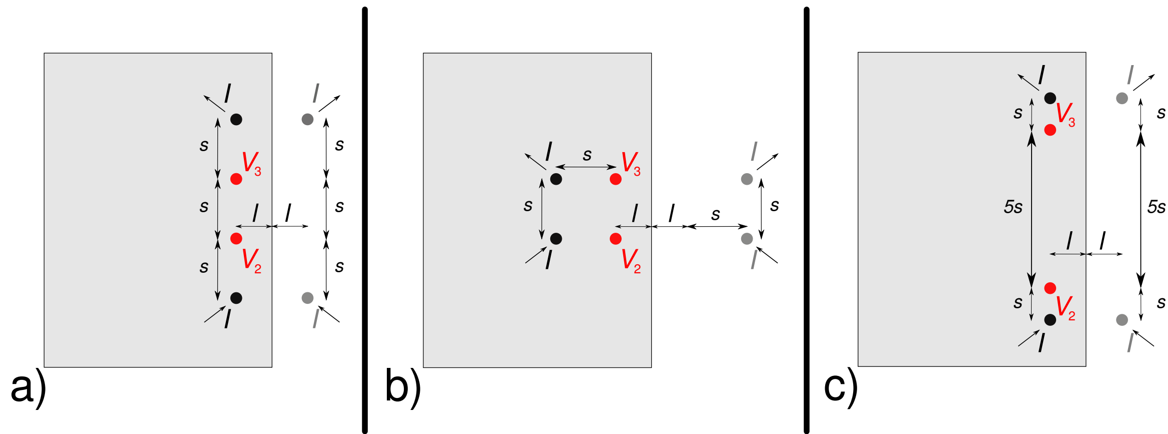

Figure 3: Sketches of the four-point probe geometries near a sample edge: a) equidistant in-line probes, b) square array probes, c) s–$5s$–s in-line probes

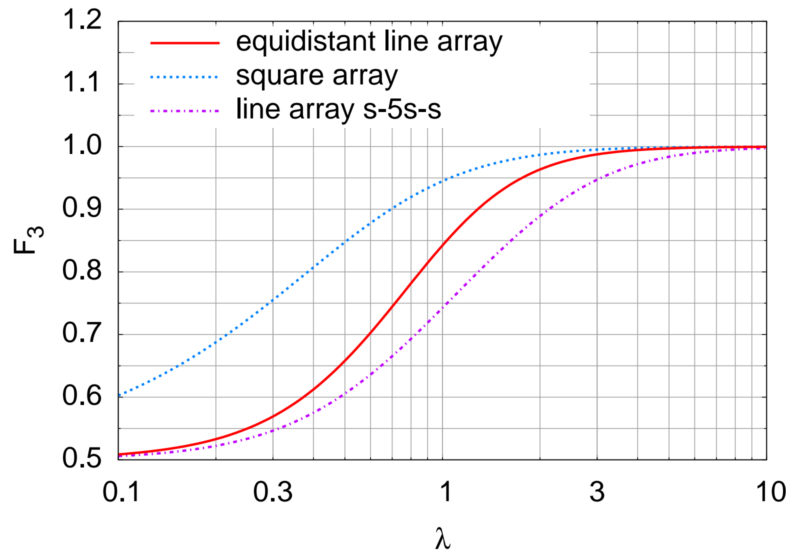

Figure 4: Correction factors F_3 for the different probe geometries as a function of the normalized distance from the edge $\lambda = l/s$ according to Eqs. (23-25)

Correction for finite lateral dimensions

We have now determined the correction factors for the finite thickness of the sample F_1 and the measurement at a sample edge F_3. The correction left is F_2 to be applied for the finite lateral dimensions. The derivation of this correction factor is as well based on the method of images and simply adding up reflected currents at all boundaries. It can be viewed in Ref. [7]. Here we do not reproduce the calculation but go on to the calculation of a single correction factor taking into account all lateral distances and the thickness of a square sample.

Combined correction factor

Since in all above cases only the superposition principle is applied it should also be possible to merge the calculations of F_1, F_2 and F_3 instead of calculating each one separately. Therefore we propose to use the method of images from the beginning in the calculation of the thickness correction factor. This means equation (13) gets additional terms from mirrored current sources (cf. Fig. 5) but the rest of the calculation stays the same. In the following we will give the most important steps in this calculation for the three geometries for the special case of a square sample where the probes are aligned parallel to one of the sides.

PAUL SCHERRER INSTITUT PSI

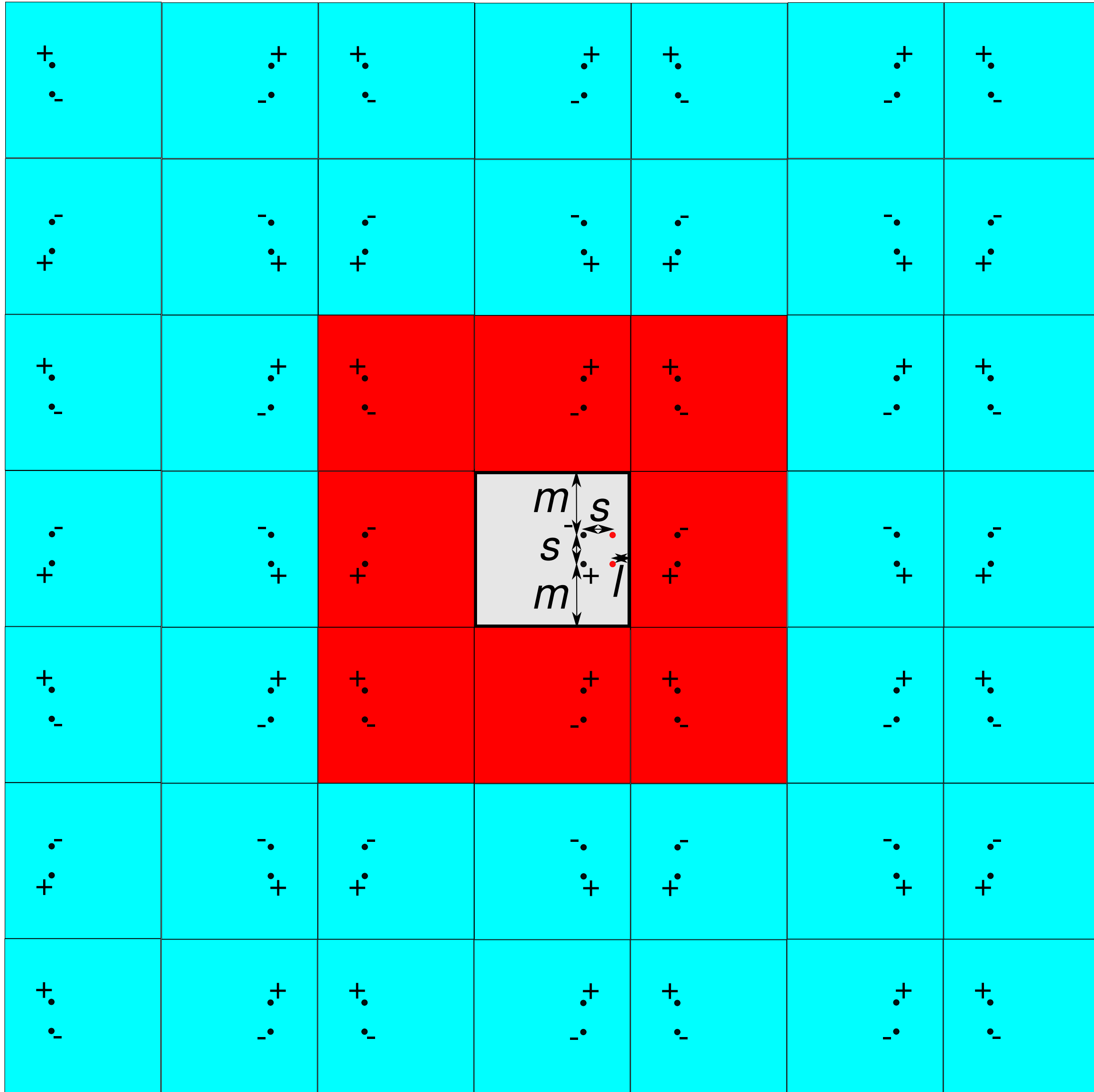

Figure 5: Sketch of the first two orders of image currents to be considered for the special case of the square probe array which is centered with respect to one side of a square sample; '+' stands for injected currents, '−' for extracted currents

Independent of the probe geometry one therefore gets

$$\Delta V(s,\tau,\lambda,\mu) = \left(\frac{\rho I}{2\pi s}\right)\left(2\int\limits_0^\infty \left\{\sum_{v=0}^{\infty}\sum_{u=0}^{\infty}\sum_{h=1}^{4}\left[\sum_{i=1}^{4} J_0\left(\kappa\sqrt{v_h(\lambda,\mu)+u_i(\lambda,\mu)}\right) - \sum_{i=5}^{8} J_0\left(\kappa\sqrt{v_h(\lambda,\mu)+u_i(\lambda,\mu)}\right)\right]\right\}\frac{\cosh(\tau\kappa)}{\sinh(\tau\kappa)}d\kappa\right) \equiv \left(\frac{\rho I}{2\pi s}\right)\tilde{f}(\tau,\lambda,\mu)\,, \tag{26}$$

where again $\tau = t/s$, $\lambda = l/s$ and $\mu = m/s$. The v_h and u_i are geometry dependent probe positions and will be given later. First we expand the series and do the integration following the recipe described in equations

PAUL SCHERRER INSTITUT PSI

(16-20) and one finally obtains

$$\tilde{f}(\tau,\lambda,\mu)=\sum_{v=0}^{\infty}\sum_{u=0}^{\infty}\left\{\sum_{h=1}^{4}\left[\sum_{i=1}^{4}\frac{2}{\sqrt{v_h(\lambda,\mu)+u_i(\lambda,\mu)}}-\sum_{i=5}^{8}\frac{2}{\sqrt{v_h(\lambda,\mu)+u_i(\lambda,\mu)}}\right]\right.$$
$$\left.+4\sum_{n=1}^{\infty}\left(\sum_{h=1}^{4}\left[\sum_{i=1}^{4}\frac{1}{\sqrt{v_h(\lambda,\mu)+u_i(\lambda,\mu)+4n^2\tau^2}}-\sum_{i=5}^{8}\frac{1}{\sqrt{v_h(\lambda,\mu)+u_i(\lambda,\mu)+4n^2\tau^2}}\right]\right)\right\}. \tag{27}$$

The v_h and u_i are given as follows:
For the equidistant in-line probe geometry

$$\begin{aligned} v_1&=(2v\delta)^2,\ v_2=(2v\delta+4\mu-2\lambda+6)^2, v_3=(2v\delta+2\lambda)^2,\ v_4=(2v\delta+4\mu+6)^2,\\ u_1&=(2u\delta-1)^2,\ u_2=(2u\delta+2\mu+5)^2, u_3=(2u\delta+2\mu+1)^2,\ u_4=(2u\delta+4\mu+7)^2,\\ u_5&=(2u\delta+2)^2,\ u_6=(2u\delta+2\mu+2)^2, u_7=(2u\delta+2\mu+4)^2,\ u_8=(2u\delta+4\mu+4)^2. \end{aligned} \tag{28}$$

For the square probe geometry

$$\begin{aligned} v_1&=(2v\delta+1)^2,\ v_2=(2v\delta+4\mu-2\lambda+1)^2, v_3=(2v\delta+2\lambda+1)^2,\ v_4=(2v\delta+4\mu+1)^2,\\ u_1&=(2u\delta)^2,\ u_2=(2u\delta+2\mu+2)^2, u_3=(2u\delta+2\mu)^2,\ u_4=(2u\delta+4\mu+2)^2,\\ u_5&=(2u\delta+1)^2,\ u_6=(2u\delta+2\mu+1)^2, u_7=(2u\delta+2\mu+1)^2,\ u_8=(2u\delta+4\mu+1)^2. \end{aligned} \tag{29}$$

For the s–$5s$–s non-equidistant inline probe array

$$\begin{aligned} v_1&=(2v\delta)^2,\ v_2=(2v\delta+4\mu-2\lambda+14)^2, v_3=(2v\delta+2\lambda)^2,\ v_4=(2v\delta+4\mu+14)^2,\\ u_1&=(2u\delta-1)^2,\ u_2=(2u\delta+2\mu+13)^2, u_3=(2u\delta+2\mu+1)^2,\ u_4=(2u\delta+4\mu+15)^2,\\ u_5&=(2u\delta+6)^2,\ u_6=(2u\delta+2\mu+6)^2, u_7=(2u\delta+2\mu+8)^2,\ u_8=(2u\delta+4\mu+8)^2. \end{aligned} \tag{30}$$

δ denotes in all cases the normalized sample width, i.e. $\delta_{\mathrm{edl}}=(2\mu+3)$, $\delta_{\mathrm{sq}}=(2\mu+1)$ and $\delta_{\mathrm{nedl}}=(2\mu+7)$. The summation of equation (27) can be done numerically and summing the first five to ten terms in u and v yields already good accuracy as can be seen in Fig. 6, where it is shown in an example how much the value of $\tilde{f}$ changes when changing the maximum order of images taken into account.

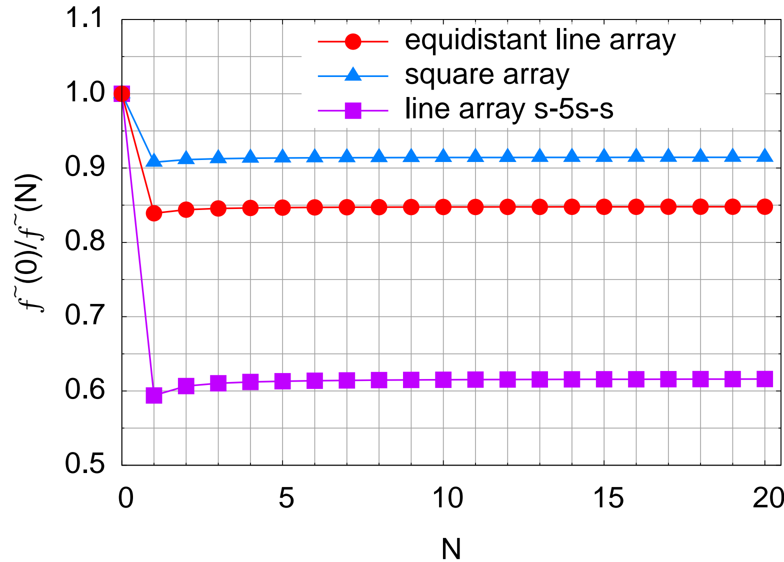

Figure 6: The geometry factor $1/\tilde{f}$ as a function of the orders of image currents taken into account for the calculation. The first three orders (0th, 1st, 2nd) are sketched in Fig. 5. The values are normalized to the value obtained involving the thickness correction only. The parameters used for these calculations are: $s=1$ mm, $t=50$ nm, $l=2$ mm, sample size 1 cm^2

Given the value of $\tilde{f}$ from (27) for one of the probe array geometries the resistivity is calculated as

$$\rho = \frac{2\pi s}{\tilde{f}(\tau,\lambda,\mu)}\frac{\Delta V}{I}\,. \tag{31}$$

Now the question arises how much the correction factor $\tilde{f}$ varies for a finite sample with a varying distance l of the probes to an edge of the sample. To investigate this behavior we look again at the example of a square sample of size 1 cm^2 and a thickness $t = 50$ nm. The probe spacing again is given by $s = 1$ mm and the first six orders of image currents are taken into account. For the three discussed probe geometries the results have been summarized in Fig. 7.

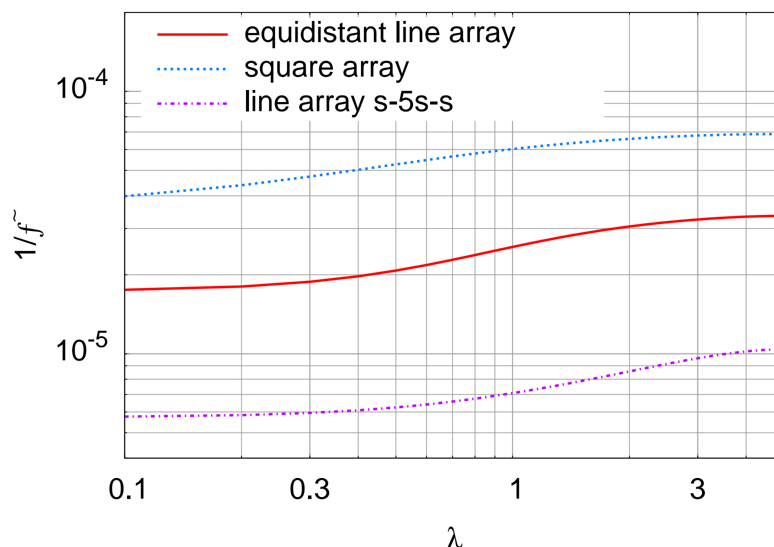

Figure 7: The geometry factor $1/\tilde{f}$ for a finite thin square sample as a function of the normalized distance to a sample edge λ. The distances to the other edges are given by the respective probe geometry and fixed. The parameters used for the calculations are: $s = 1$ mm, $t = 50$ nm, $N = 6$, sample size 1 cm^2

Finally we have a look at the thickness dependence of the correction factor $1/\tilde{f}$ and provide a practical formula for each studied probe geometry which might be used for data analysis if always the same sample and probe geometry is used and only the thicknesses of the samples vary. Since in our case most of the investigated thin film samples have the standard size of 10 mm × 10 mm and the probe distance is $s = 1$ mm, we have done the calculations for this sample size and probe spacing. Fig. 8 shows the t-dependence of the overall correction factor $1/\tilde{f}$. Also here we have used a fixed distance to the edge of $l = 2$ mm as an input to the calculations and have taken into account the first six orders of image currents.

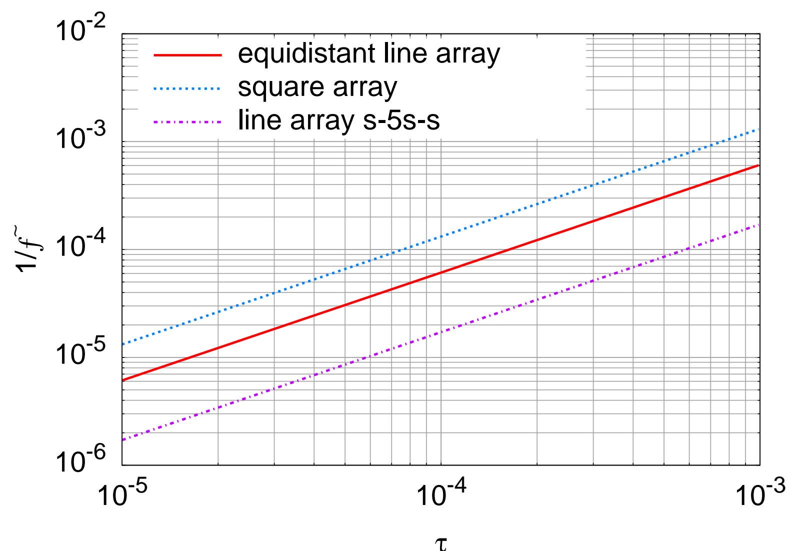

Figure 8: The geometry factor $1/\tilde{f}$ for a finite thin square sample as a function of the normalized sample thickness $\tau = t/s$. The parameters used for the calculations are: $s = 1$ mm, $l = 2$ mm, $N = 6$, sample size 1 cm^2

From a fit to the data shown in Fig. 8 we obtain the resistance-resistivity-conversion factor for thin homogeneous films, where the square sample has the size of 1 cm^2. The probe spacing is $s = 1$ mm and each probe array is placed $l = 2$ mm away from the edge parallel to the line connecting the voltage contacts and is centered with respect to this sample side.

$$\begin{aligned}\rho\,[\mathrm{m}\Omega\mathrm{cm}] &= 3.83916 \times 10^{-4} \cdot t\,[\mathrm{nm}] \cdot R_{\mathrm{edl}}\,[\Omega] \\ &= 8.28303 \times 10^{-4} \cdot t\,[\mathrm{nm}] \cdot R_{\mathrm{sq}}\,[\Omega] \\ &= 1.07616 \times 10^{-4} \cdot t\,[\mathrm{nm}] \cdot R_{\mathrm{nedl}}\,[\Omega]\end{aligned} \tag{32}$$

References

[1] D. K. Schroder, *Semiconductor Material and Device Characterization*, 3rd ed. (Wiley, New Jersey, 2006), chapter 1

[2] R. A. Weller, *An algorithm for computing linear four-point probe thickness correction factors*, Rev. Sci. Instrument. **72** (2001) 3580-3586

[3] L. B. Valdes, *Resistivity Measurements on Germanium for Transistors*, Proc. IRE **42** (1954) 420-427

[4] J. Albers and H. L. Berkowitz, *An Alternative Approach to the Calculation of Four-Probe Resistances on Nonuniform Structures*, J. Electrochem. Soc. **132** (1985) 2453-2456

[5] S. B. Catalano, *Correction Factor Curves for Square-Array and Rectangular-Array Four-Point Probes Near Conducting or Nondonducting Boundaries*, IEEE Trans. Electron. Devices, **10** (1963) 185-188

[6] A. Uhlir, Jr., *The Potentials of Infinite Systems of Sources and Numerical Solutions of Problems in Semiconductor Engineering*, Bell Syst. Tech. J., **34** (1955) 105-128

[7] F. M. Smits, *Measurement of the Sheet Resistivities with the Four-Point Probe*, Bell Syst. Tech. J., **37** (1958) 711-718